J Mater Sci: Mater Med (2013) 24:2001–2011
DOI 10.1007/s10856-013-4956-8

Host reaction to poly(2-hydroxyethyl methacrylate) scaffolds in a small spinal cord injury model

Hong Ying Li · Tobias Führmann · Yue Zhou · Paul D. Dalton

Received: 11 March 2013 / Accepted: 7 May 2013 / Published online: 24 May 2013

Abstract Tissue engineered scaffolds and matrices have been investigated over the past decade for their potential in spinal cord repair. They provide a 3-D substrate that can be permissive for nerve regeneration yet have other roles including neuroprotection, altering the inflammatory cascade and mechanically stabilizing spinal cord tissue after injury. In this study we investigated very small lesions (approx. 0.25 μL in volume) of the dorsal column into which a phase-separated poly(2-hydroxyethyl methacrylate) hydrogel scaffold is implanted. Using fluorescent immunohistochemistry to quantify glial scarring, the poly(2-hydroxyethyl methacrylate) scaffold group showed reduced intensity compared to lesion controls for GFAP and the chondroitin sulfate proteoglycan neurocan after 6 days. However, the scaffold and tissue was also pushed dorsally after 6 days while the scaffold was not integrated into the spinal cord after 28 days. Overall, this small-lesion spinal cord injury model provided information on the host tissue reaction of a TE scaffold while reducing animal discomfort and care.

H. Y. Li · Y. Zhou (✉) · P. D. Dalton
Med-X Research Institute, Shanghai Jiao Tong University, 1954 Huashan Rd, Shanghai 200030, China
e-mail: yzhou2009@sjtu.edu.cn

H. Y. Li · Y. Zhou
School of Biomedical Engineering, Shanghai Jiao Tong University, 1954 Huashan Rd, Shanghai 200030, China

T. Führmann · P. D. Dalton (✉)
Institute of Health and Biomedical Innovation, Queensland University of Technology, 60 Musk Ave, Kelvin Grove, QLD 4059, Australia
e-mail: daltonlab@gmail.com

1 Introduction

The loss of function after spinal cord injury (SCI) is due to the destructive consequences of the primary injury combined with the subsequent cascade of pathophysiological events, termed secondary degeneration, which includes complex inflammatory events [1, 2]. Due to the complexity of the pathophysiological events and the variety of types of injury (e.g. compression/contusion, laceration and transection), many conceptual different treatment strategies have been investigated, including drug-, cell- and biomaterial-based strategies [3–5]. Depending on the treatment strategy, various SCI models have been used, including contusion-type injury models such as the New York University weight-drop device [6–8], the infinite horizon impactor [9] and the electromagnetic spinal cord injury device (ESCID) [10], as well as balloon [11] and clip compression models [12]. These models are associated with a significant and measured loss of function [6–8, 13]. This loss in locomotor function can determine the effectiveness of a therapy to some extent, but requires labor and cost intensive animal care.

Biomaterial-based treatment strategies most commonly investigate experimental animal models in which part of the spinal cord is resected to have physical space to transplant scaffolds/hydrogels. Many different matrices and tissue engineering (TE) scaffolds have been implanted including hydrogels such as fibronectin [14, 15], fibrin [16], pHEMA [17–19], or agarose [20, 21]. Such in vivo studies of TE scaffolds/matrices focus mainly on their capacity to support axonal regeneration [14, 15, 17, 20, 21], or transplant cells [16, 22]. However, implanted scaffolds potentially alter the injury cascade and affecting secondary injury as well as gliosis [17]. Emphasizing that scaffolds can provide more than a regenerative substrate for axons or a vehicle for cell transplantation, fibronectin recently

demonstrated neuroprotective properties in addition to promoting regeneration [14]. Such hemi-section models remain difficult to translate into the clinic as spinal cord tissue is resected or aspirated out of the area. Nonetheless there are scientific elements in hemi-section models that are important to investigate, including improving our understanding of tissue response and material integration into the spinal cord. For example, an intramedullary implant model has been recently used to assess biocompatibility and long-term (1 year) degradation, using thin pieces of a biomaterial [23]. Such approaches using smaller injuries—even though they are not clinically relevant—might assist fundamental understanding of biomaterial integration while reducing animal discomfort and care.

While many models generally focus on axonal regeneration, in this study we aim to understand the early tissue response after injury (6 days), and how this is affected by the implantation of a TE scaffold. To contribute to our understanding of how the scaffold affects the surrounding tissue, acute implantations into small injuries of white matter tracts of the dorsal column were investigated. Our analysis focused on the astrocytic response, specifically GFAP, and the distribution of neurocan—a chondroitin sulfate proteoglycan (CSPG) that prevents axonal regeneration, both which were down-regulated at the injury site after pHEMA implantation. The small lesion SCI model described in this study minimizes both the injury and post-operative care and is aimed at studying tissue response to the TE scaffold rather than being clinically relevant.

2 Materials and methods

2.1 Materials

All chemicals were purchased from Sigma Aldrich (China) unless otherwise indicated. The monomer, 2-hydroxyethyl methacrylate (#477028), was 99 % purity and used as received, while the PCL (#440744) had a molecular weight of 70,000–90,000 g/mol. Methanol (99.5 % purity; #100 14118), chloroform (99 % purity; #10006818) and H_2O_2 (30 % solution; #10011208) were sourced from SCRC (China). Tetramethylethylenediamine (TEMED) (#AMR-0761) was purchased from Mandel Scientific Company Inc., (Canada). Hypnorm (0.05 mg/mL) and Hypnovel (1 mg/mL) were purchased from Yichang Humanwell Pharmaceutical Co., Ltd., (China) and Nhwa Pharma Corporation (China) respectively.

2.2 Electrospinning

An artificial dura to be positioned between the exposed spinal cord and dorsal muscle tissue was made by electrospinning PCL using established formulations [24] and methods [25]. Briefly, a 10 wt% PCL solution (75/25 vol.% chloroform/methanol) was electrospun for 5 min onto a single aluminum foil collector, with a collector distance of 10 cm, flow rate of 0.5 mL/h and applied voltage of 10 kV.

2.3 Hydrogel scaffold

The pHEMA hydrogel scaffold was produced by phase-separating HEMA through polymerization in excess water [17, 26]. Briefly, 931 μL of HEMA was mixed with 4.67 g H_2O and 45.6 μL of a 10 % APS solution and cooled in a refrigerator. TEMED (5.2 μL) was added and a total of 0.5 mL of the solution was injected through a 0.22 μm PTFE filter into a sterile 1 mL syringe. After 1 h of polymerization in the refrigerator, the syringes were removed and kept at room temperature overnight. Thin slivers (approximately 0.2 mm) were sliced off the pHEMA scaffold under a stereomicroscope using a no. 10 scalpel and UV sterilized.

2.4 Scanning electron microscopy

Both the pHEMA scaffold and electrospun PCL were imaged with scanning electron microscopy (SEM). The pHEMA scaffold was frozen at −20 °C, then sections of the hydrogel cut using a scalpel. These pieces were placed in a 15 mL Falcon tube and frozen further in liquid nitrogen and lyophilized overnight. The lyophilized and electrospun PCL mesh were mounted on stubs and sputter coated with gold before being imaged (Quanta 200 scanning electron microscope, FEI). A working distance of 13 mm and 10 kV were used to view the samples. Fiber diameters of the electrospun PCL mesh were measured by randomly imaging three different regions of the mesh, followed by averaging 20 fibers per image ($n = 60$ in total).

2.5 Surgery

The investigations were performed at the Med-X research institute (Shanghai Jiao Tong University, China) and were subject to the local ethics committee permission. Young adult male Wistar rats (230–260 g; $n = 5$ for each group) were used for the in vivo study. Body temperature under anesthesia was regulated with a heated mat while surgery itself performed using a surgical microscope (M651 MSD, Leica). Under Hypnorm/Hypnovel (2 mL/1.6 mL) injection anesthesia/analgesia, the back of the rodent was shaved and the skin sterilized with 70 % alcohol prior to a 2–3 cm incision along the midline, approximately above T5/T10. Using blunt dissection, the superficial muscle layers were cleared from the deeper layers, a midline

incision was made and the superficial and deep muscle layers retracted to expose the dorsal surface of the T6–T8 vertebrae. Fine bone rongeurs (16021-14, Fine Science Tools, Germany) were used to perform a laminectomy of the T7 vertebra, exposing the dorsal surface of the spinal cord. The dura was cut and reflected with the sharp edge of a beveled 26G needle tip (#301321, BD Biosciences), after which a 0.2 mm (rostral/caudal) × 0.3 mm (bilateral) section of the cord was identified on the dorsal column (Fig. 1) that minimized disruption of the spinal cord vasculature. A bilateral transverse incision was made in the dorsal column of the spinal cord, excising out to a depth of approximately 0.4 mm. A sliver of pHEMA scaffold was placed next to the injury site and cut into a shape approximately 0.2 mm × 0.3 mm × 0.4 mm in size (0.24 μL). The scaffold was fitted into the lesion area, minimizing the pressing down of the material into the spinal cord. For lesion only controls, the scaffold was not placed into position. For both the lesion only and pHEMA scaffold groups, the PCL electrospun membrane was placed over the exposed site, acting as a fine barrier to minimize the infiltration of fibroblasts into the SCI parenchyma [27, 28]. The skin was closed using 4/0 coated Vicryl-plus antibacterial sutures (VCP773D, Ethicon, USA) and animals were socially housed on irradiated sawdust, 2 animals/cage, in type RU polysulfone cages (420 × 250 × 230 mm) as part of a rack-based ventilation system (RU25S7-2, Suhang Technologies, China). Animals had access to water ad libitum with a 12:12 h light regime. The following day, all animals moved freely in their cage, fed and drank without any indication of pain or discomfort. Animals were sacrificed 6 and 28 days after injury.

2.6 Animal preparation for IHC analysis

Terminal anesthesia was induced with an intra-peritoneal overdose of ketamine (200 mg/mL; 1.5–2 mL). The animal was then transcardially perfused with 0.9 % heparinized saline followed by 10 % formalin buffered saline (FBS). After approximately 2–3 min of perfusion (approx. 40–60 mL), the injured part of the spinal cord was dissected out and then post-fixed in FBS for 24 h. The spinal cord was embedded in paraffin wax (Leica EG 1160) and sagittal sections of 10 μm in thickness (Leica, RM2245) were taken throughout the areas of interest, including the pHEMA scaffold and the surrounding tissue.

2.7 Histology and immunohistochemistry

After fixation and embedding, samples were processed for both histological and immunohistochemical staining as described previously [29]. Paraffin-embedded sections underwent sequential solvent exchange from xylene to 100 % ethanol to ethanol mixtures to PBS. The sections were quenched using a 0.3 % H_2O_2 methanol solution, and then heat-mediated antigen retrieval in 10 mM citrate buffer was performed. Primary antibodies were diluted in PBS with 10 % goat serum and incubated with the preparations at room temperature for 45 min. Uninjured spinal cords were stained with luxol fast blue, which identifies myelin and was used to provide a schematic in Fig. 1.

To identify the maximum injury site, activated macrophages and microglia were identified using a monoclonal antibody against CD68 (1:200, ED-1, MCA341R, Serotec, USA) [29]. Glial fibrillary acidic protein (GFAP) was detected with a polyclonal antibody (1:2000, Z0334, DAKO, USA) while neurocan was identified with a monoclonal antibody (1:2000, ab26003, Abcam, USA). Primary antibodies were detected by biotinylated secondary antibodies (1:200 dilution, #BA-1000 and 2000, Vector Laboratories, USA). These sections were cover-slipped with Vectorshield mounting medium with DAPI (Vector Laboratories, USA) and imaged immediately. For non-fluorescent immunohistochemistry (IHC) of ED-1, antibody

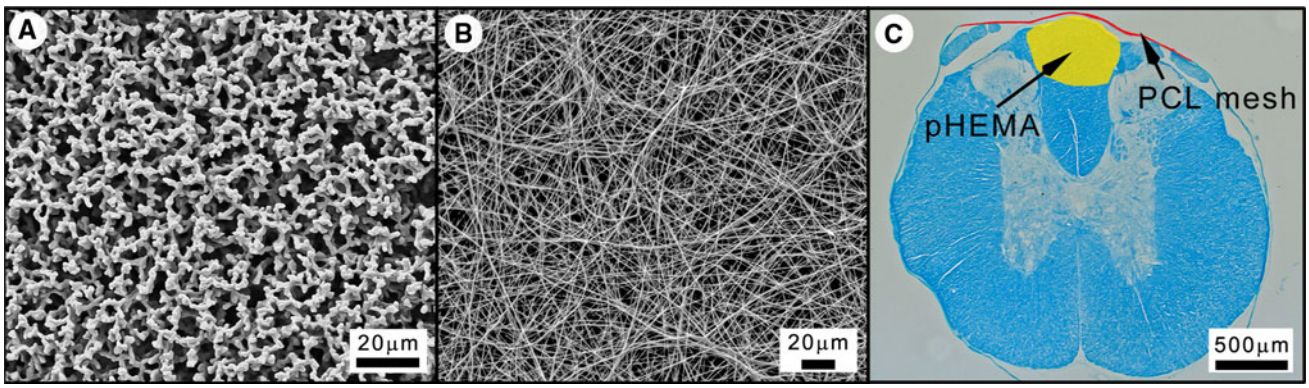

Fig. 1 SEM images of the (**a**) pHEMA scaffold implanted in the dorsal column of the spinal cord and (**b**) electrospun non-woven PCL mesh used to cover the exposed spinal cord after surgery. (**c**) A transverse section of the spinal cord stained with luxol fast blue (*myelin*) with an overlay approximately indicating the injured region (*yellow*) and the location of the PCL mesh (*red*) in false color (Color figure online)

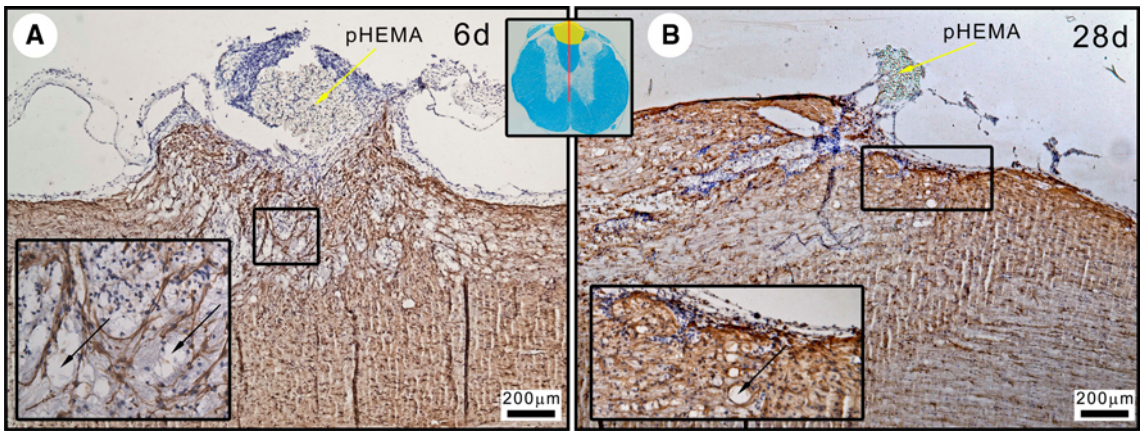

Fig. 2 Sagittal sections of spinal cords 6 days (**a**) and 28 days (**b**) after receiving a pHEMA implant and immunostained for GFAP. The pHEMA scaffold (*yellow arrow*) is dorsally pushed due to localized oedema, or swelling of the spinal cord, and is entirely pushed out after 28 days. Microvacuolation of the spinal cord can be seen and are indicated with *black arrows* within the inset images. Between, a transverse section of an injured spinal cord with the sagittal plane and injured area is indicated. The electrospun PCL mesh cannot be visualized as it is dissolved during the embedding process (Color figure online)

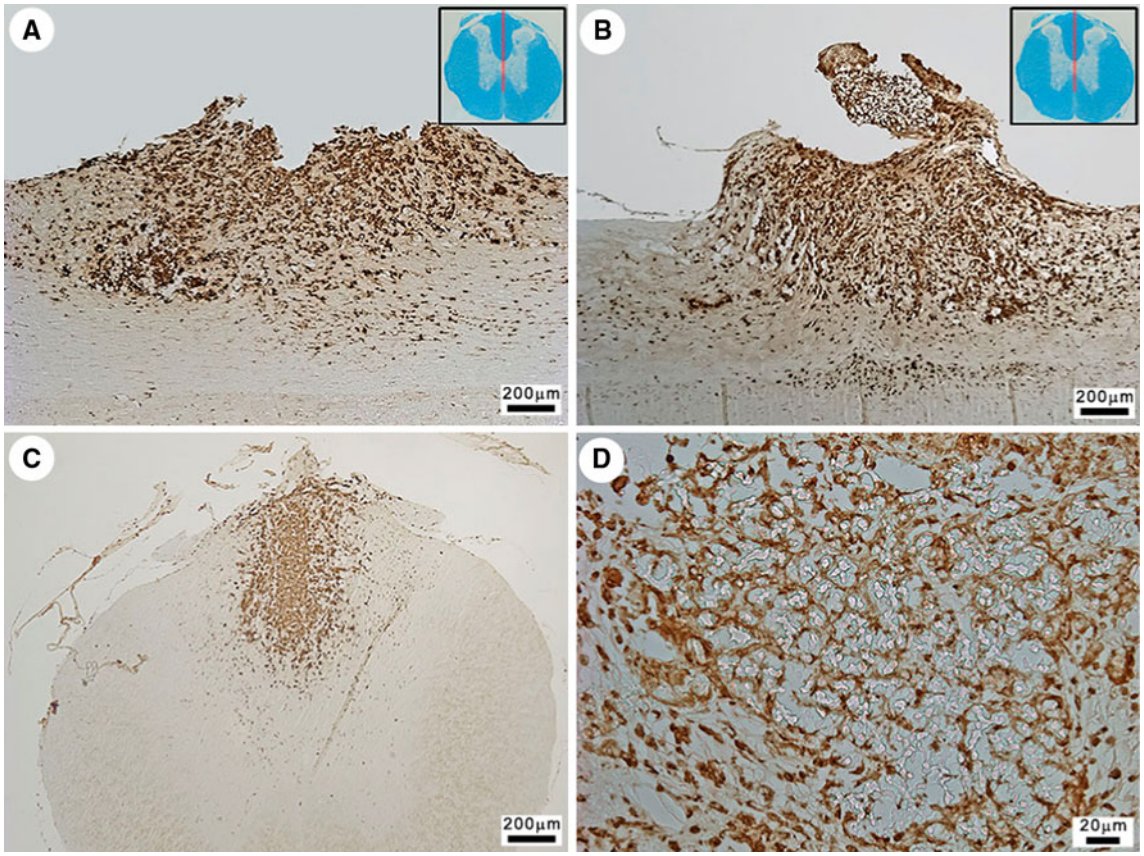

Fig. 3 ED-1+ cells surround the injury site and penetrated the pHEMA scaffold. Spinal cord sections stained for ED-1 to identify activated macrophages and microglia. Saggital sections of (**a**) lesioned and (**b**) scaffold-implanted spinal cords show a similar recruitment of these phagocytic cells. (**c**) Transverse section of the injury site demonstrates that the lesion is within the dorsal funiculus. A magnified view of the scaffold (**d**) shows it filled with ED-1+ cells. To prevent interference by similar colored chromogens, the nuclei were not counterstained. *Insets* in (**a**) and (**b**) show the section plane

binding was visualized with avidin–biotin–peroxidase complex (ABC) (Vector Laboratories, USA) and 3,3′-diaminobenzidine tetrahydrochloride used as a chromogen. These sections were then sequentially dehydrated from ethanol into xylene, followed by embedding with DPX (#44581, Sigma Life Science), and left to dry overnight.

2.8 Evaluation

Using ImageJ (NIH, USA), the green (GFAP) or red (neurocan) fluorescent images were converted to a grey-scale image and the mean grey value (intensity) used for quantification. An approximate threshold was visually set that only included the GFAP+ signal while excluding the background. This threshold methodology was repeated 3 times/animal, with 4 animals/group studied, using slides next to the area of greatest ED-1 immunofluorescence. Using the ventral side intensity as a control we compared the GFAP+ signal (intensity/region) within a 2 mm (rostral/caudal) × 0.5 mm rectangle centered on the injury area. Each GFAP+ intensity measurement (intensity/region) was normalized to an uninjured area of the dorsal column to minimize any sample-to-sample fluorescent staining variations.

For measurement of the spatial distribution of neurocan across the injury site, a box was overlaid on the injury site and separated in 200 × 500 μm areas. Each neurocan intensity measurement (intensity/region) was normalized to an uninjured area of the dorsal column to minimize any sample-to-sample fluorescent staining variations. Statistical tests for the GFAP and neurocan analysis were performed using MS Excel software. An unpaired student *t* test was performed between each groups (normal, lesion and pHEMA) using a two-tailed test to determine statistical significance ($P \leq 0.05$).

3 Results and discussion

Biomaterial-based intervention strategies for bridging SCI aim to replace damaged tissue with an axon growth promoting substrate, which is able to integrate within the host tissue. A range of different TE scaffolds have been implanted in vivo using hemi-section injury models, the majority of these disrupting a significant portion of the spinal cord (scaffold volume 10–180 μL; median 36 μL) and involving a loss of function [14, 17, 20, 21, 23, 30–36]. In the current study, a smaller volume of a TE scaffold was implanted (approx. 0.25 μL); the objective was to investigate the integration and the surrounding microenvironment

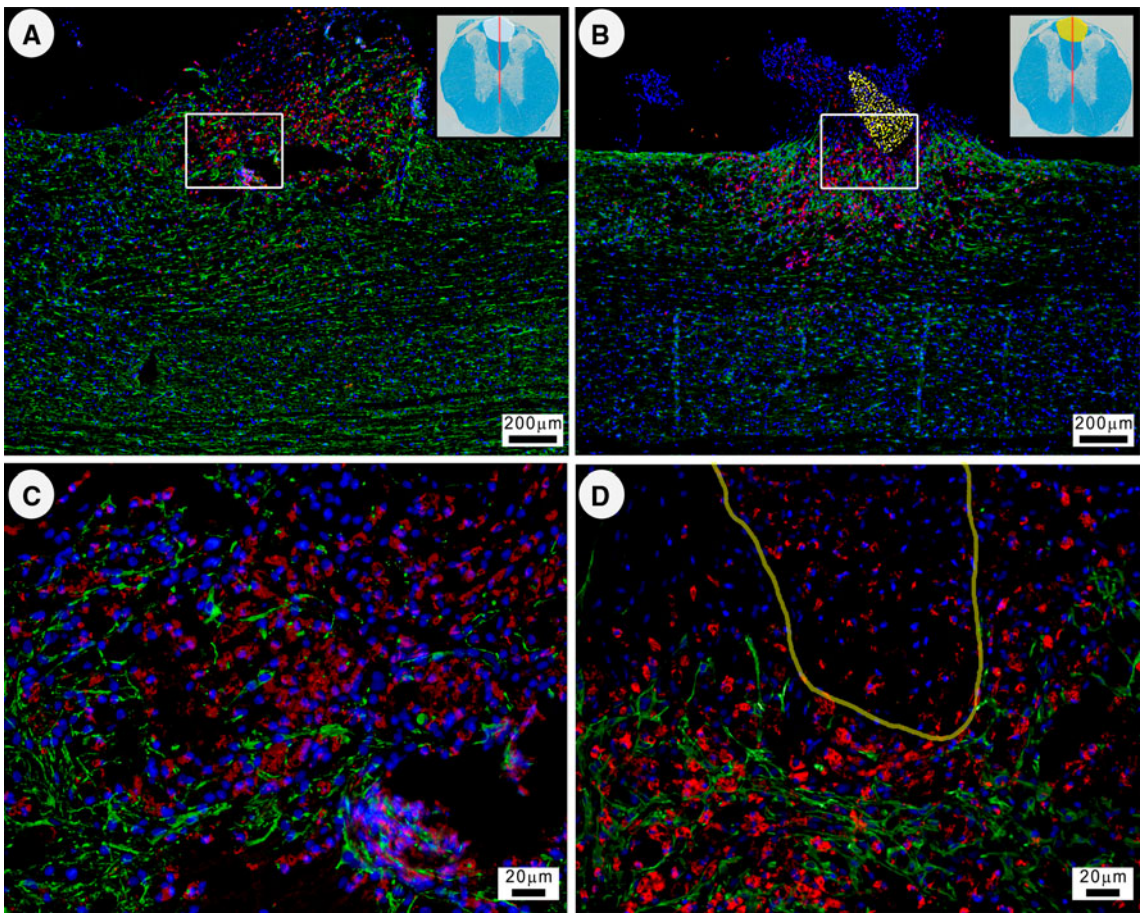

Fig. 4 Sagittal sections of the spinal cord showing lesion only spinal cord (**a** and **c**) and scaffold implanted tissue (**b** and **d**). Activated macrophages/microglia (ED-1+; *red*), astrocytes (GFAP+; *green*) and cell nuclei (DAPI+; *blue*) are shown. Since the pHEMA scaffold is not visible under fluorescence, bright-field images were also obtained and the scaffold either false colored *yellow* (**b**) or outlined (**d**) (Color figure online)

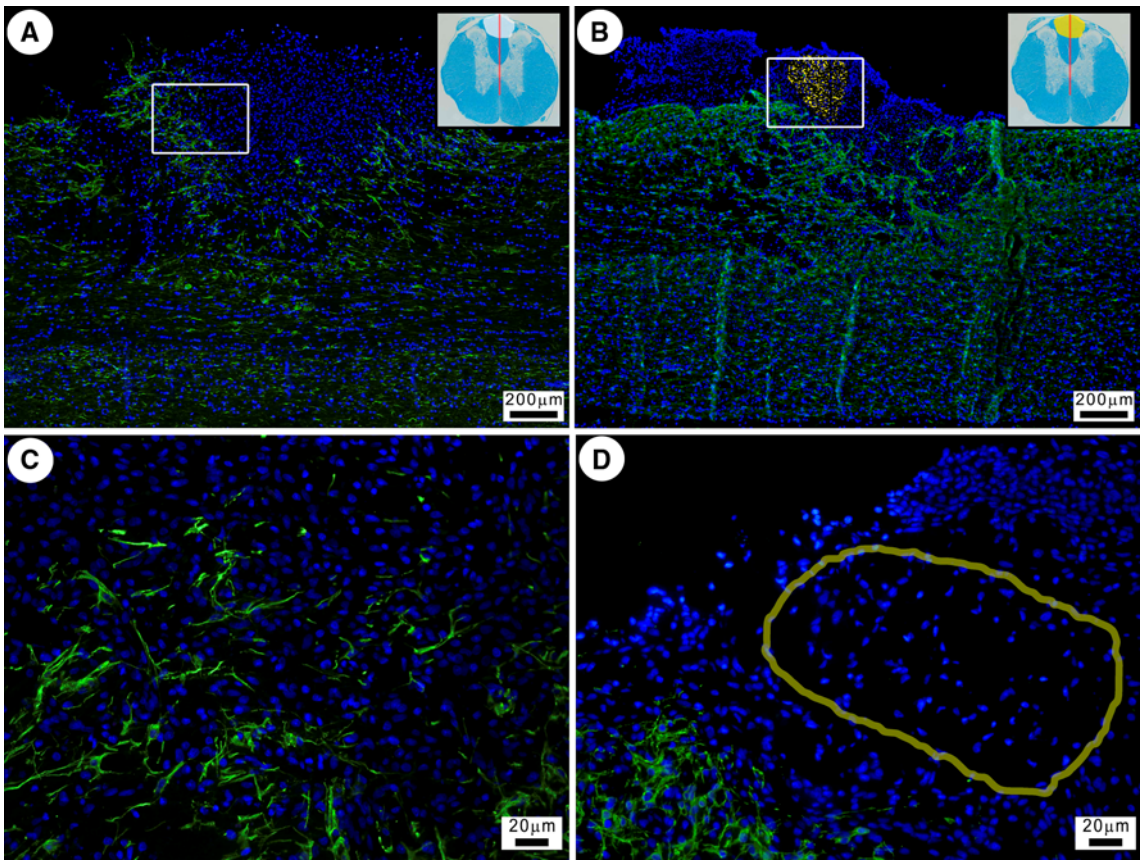

Fig. 5 Sagittal sections of the spinal cord showing that the pHEMA scaffold implantation affects GFAP intensity at the lesion site. Host astrocytes (stained for GFAP, *green*) surround the injury site of control (**a**) and scaffold implanted (**b**) animals. Nuclei were counterstained with DAPI (*blue*). Higher magnification images of the lesion site in control (**c**) and scaffold implanted (**d**) animals. The pHEMA scaffold outline is highlighted in (**d**) (Color figure online)

of such scaffolds while minimize loss of function to the animal. Additionally this surgical model disrupts the white matter tracts of the dorsal column only, while other hemi-section studies in cause damage to both white and grey matter. A relatively short post-surgery time point of 6 days was used for analyzing the inflammatory reaction while tissue was taken at 28 days to observe integration after longer survival times to determine regenerative potential.

The choice of species, strain, sex and age (rat; Wistar; male; young adult) is meant to minimize some of the fluctuations that can occur after SCI. Male animals are preferred over females as the latter have fluctuations in oestrogen levels, which could affect the response to SCI [37, 38]. The animals undergoing this SCI model required no manual bladder expression and had minimal loss of function. Each surgery took approximately 45–60 min, depending on the extent of bleeding. The pHEMA hydrogel scaffold fitted readily into the lesion site and fixation was assisted with fibrin clot formation due to blood vessel

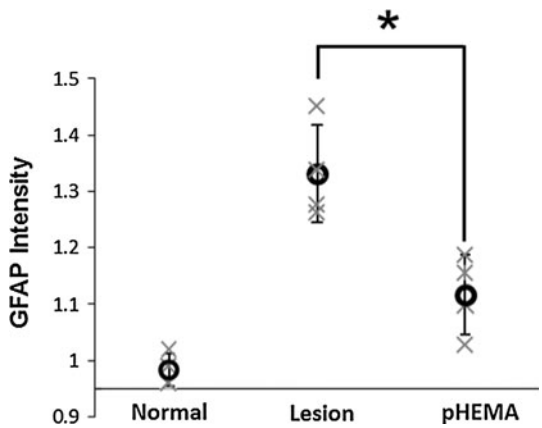

Fig. 6 Evaluation of the GFAP immunoreactivity shows that scaffold implantation reduced reactive gliosis. GFAP intensity measurement comparing an area measuring 2 mm × 0.5 mm over the injured or scaffold area. This GFAP intensity is a ratio generated by dividing the fluorescent intensity of the injured area with fluorescence of the ventral white matter. The pHEMA group is also statistically significant to normal controls

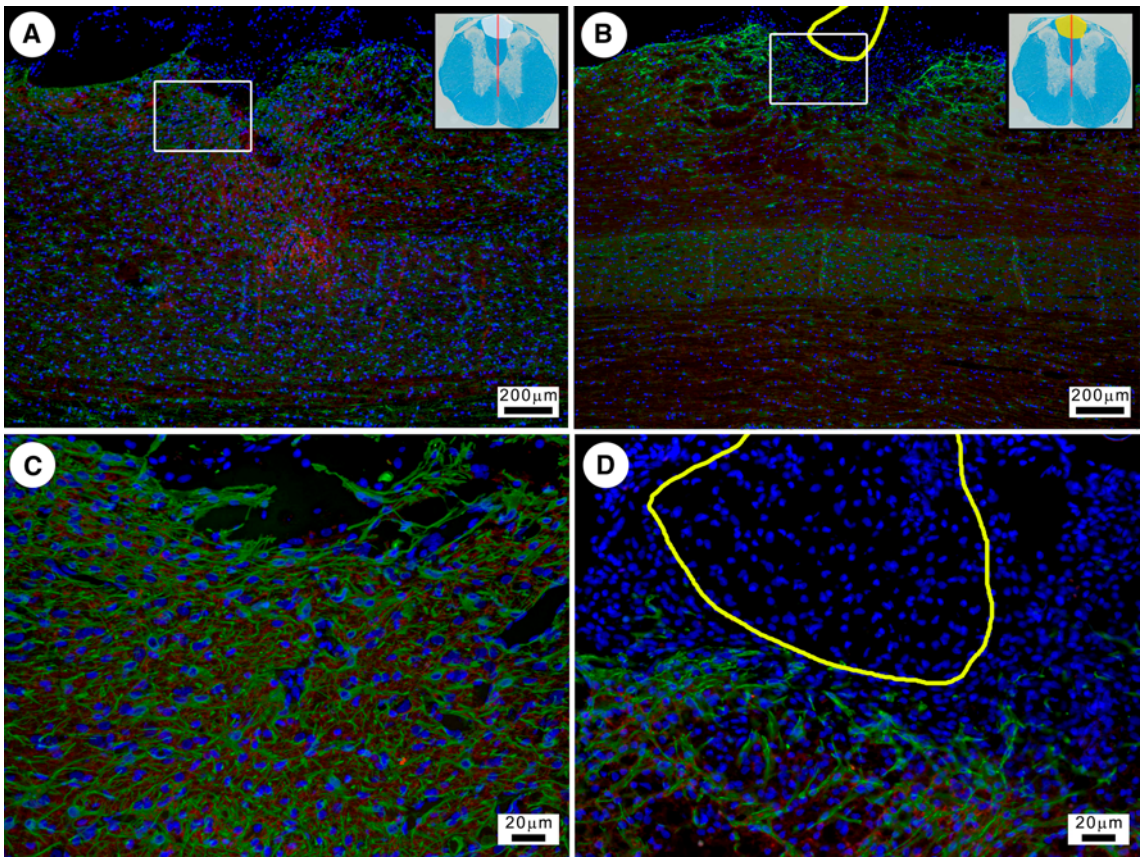

Fig. 7 IHC images showing that neurocan expression is different between control and scaffold groups. Neurocan (*red*) is up-regulated significantly ventral to the injury for controls (**a** and **c**) while the fluorescent signal for both groups is increased rostral/caudal of the injury. Astrocytes are stained for GFAP (*green*) while nuclei were counterstained with DAPI (*blue*). Higher magnification images of the lesion in control (**c**) and scaffold implanted (**d**) animals with the pHEMA scaffold outlined in (**d**) (Color figure online)

disruption. Figure 1a shows a SEM image of the pHEMA scaffold, which has open, interconnected pores for cell invasion. The electrospun PCL membrane (shown in Fig. 1b) fitted well to the dorsal surface of the spinal cord. SEM measurements showed that the electrospun membrane had an average fiber diameter of 480 ± 170 nm. We chose to implant a non-degradable scaffold, based upon pHEMA, to establish this small lesion model of the spinal cord. A degradable TE scaffold could release products that influence the microenvironment surrounding the implant, which is not desired in establishing this small lesion model. Furthermore, this phase-separated hydrogel scaffold has a history of biomedical use [17, 39, 40], in more severe SCI models. PHEMA scaffolds can also be readily surface modified and morphology altered to improve their regenerative properties in the spinal cord [18].

In this small lesion model a dorsal relocation of the pHEMA scaffold occurred after 6 days (Fig. 2a), accompanied by localized oedema, or swelling, of the spinal cord, which occurs naturally shortly after injury [41]. This oedema was observed in both scaffold and lesion groups. At 28 days, the pHEMA scaffold was even more dorsally relocated and it was difficult to find in spinal cord tissue (Fig. 2b). Since pHEMA is not considerable biodegradable, its absence in the spinal cord sections indicates that it was dorsally pushed out of the tissue. It would be important to understand whether reconstructing the dura as a mechanical barrier will assist or inhibit scaffold integration, including scarring and ECM production. In this small lesion model, the pia/dura was not reconstructed to mechanically prevent the scaffold from being dorsally relocated. Instead an electrospun PCL non-woven mesh was placed over the dorsal column, which provides a cell-impermeable membrane that does not mechanically hold the scaffold into place. Reconstructing the dura in this instance would involve suturing the damaged membrane, providing a mechanical barrier that prevents the oedema from dorsally relocating the spinal cord tissue. This approach of using a mechanical barrier could result in further damage to the spinal cord, as the swollen injured region compresses surrounding tissue. Even though the injured tissue/scaffold was pushed dorsally, the microenvironment surrounding the implant and lesion could still be investigated for the 6 days time point. While our goal is to

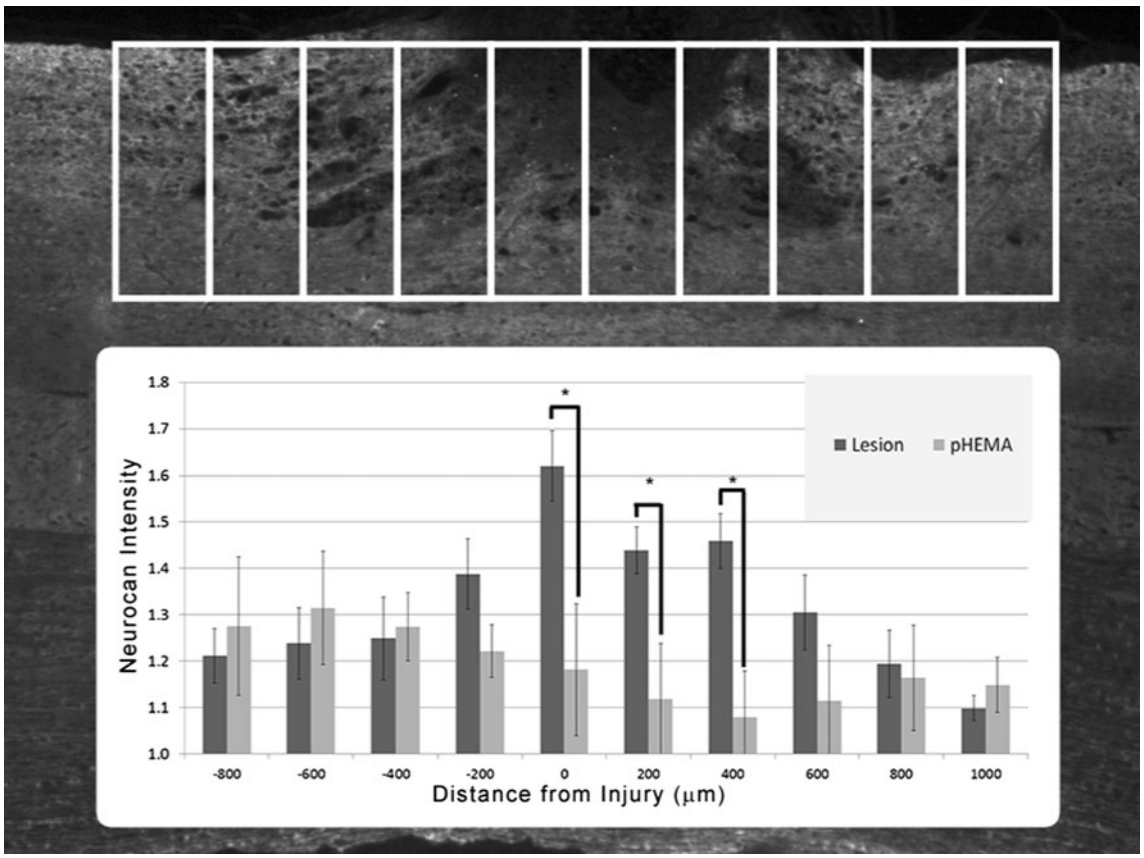

Fig. 8 Calculation and comparison of neurocan expression in both the scaffold and control group. The *graph* shows the comparison of neurocan intensity (average intensity/area) between control and scaffold groups, with significantly different intensities at 0, 200 and 400 μm ($P \leq 0.05$). The spinal cord section shown in this example is from the pHEMA scaffold group

establish a small lesion SCI model for TE scaffold integration, the robust dorsal relocation of the scaffold indicates that unmodified pHEMA may not be well-suited for regeneration in this tissue.

3.1 Immune response

Since SCI is partly driven by inflammatory processes, we used ED-1 (CD68) staining to determine the center of the injury so that GFAP and neurocan assessments can be made at the sites of maximum injury. The ED-1 antibody stains activated macrophages and microglia; fluorescent and light micrographs are shown in Figs. 3 and 4 respectively. As can be seen in Fig. 3a, b, the injury center, immediate parenchyma and the dorsal surface contain the majority of ED-1+ cells while the pHEMA scaffold was filled almost exclusively with ED-1+ cells (Fig. 4d). Quantitative analysis of ED-1+ cells was not accurately possible, as the tissue dorsal to the injury is structurally weak and does not adhere well to the slides, with some lifting off during IHC processing. Since this region contains a significant amount of ED-1+ cells, we were unable to accurately quantify and compare the ED-1 response between the scaffold and lesion groups. Therefore ED-1 was only used qualitatively to describe activated macrophage/microglia distribution and detect the lesion epicenter for the GFAP and neurocan measurements. The transverse tissue section shown in Fig. 3c provides a different perspective of the injury response, and the surgery. The extent of ED-1+ cells could be found well beyond the depth of the lesion (0.3 mm).

3.2 Reactive gliosis

The extent of reactive gliosis in the injury parenchyma was measured through GFAP intensity of fluorescently stained sections (Fig. 5). GFAP, which is an intermediate filament within astrocytes, is commonly known to be up-regulated after injury and a measure of gliosis [42, 43]. However the role that such intermediate filaments play in the mechanical stabilization of CNS tissue is only recently being understood. A recent article showed that an increase in the intermediate filaments of astrocytes correlates with the stiffness of the tissue [44] providing a mechanical barrier to axon regeneration. In this study, no GFAP labeled filaments can be seen within the injury area of either group, while GFAP is clearly elevated compared to

the rest of the cord in the injury parenchyma. There was no GFAP signaling seen within the pHEMA scaffold (Fig. 5d) indicating no migration of host astrocytes into this region. Furthermore, the pHEMA group had a significantly lower ($P = 0.008$) GFAP signal surrounding the implant area (Fig. 6) compared to lesion control animals. As would be expected, the pHEMA group had a statistically higher ($P = 0.01$) average GFAP+ intensity than uninjured controls.

One possible explanation to the lower GFAP expressions is that the scaffold rapidly stabilizes the spinal cord mechanically, before being pushes out by the oedema, reducing the need for the astrocytes to arrest the extent of injury. Since scaffolds are a porous material, endogenous fibrin clots assist in mechanical stabilization through interlocking the scaffold pores with the natural tissue. Figure 5d shows a magnified image of the pHEMA implant with astrocytes that are approximately 50 μm away from the pHEMA scaffold. Qualitatively, this compares to the lesion controls where there is a more extended loss of GFAP signal around the injury foci. The implantation of cell-invasive scaffolds has shown a reduction in cystic cavity formation in other studies including those with poly(hydroxypropyl methacrylamide) [45], fibronectin [15], collagen [46–48], and poly(lactide-co-glycolide) [22]. Such scaffolds allow the infiltration and bonding with spinal cord tissue, possibly reducing the need for astrocytes to form a dense scar that later prevents regeneration. The mechanical stabilization of the injured spinal cord by using injectable hydrogels or scaffolds has a significant potential for research.

3.3 Distribution of neurocan extracellular matrix

Neurocan is an axon growth inhibitory CSPG that is produced by astrocytes and is up-regulated after injury to the CNS [49, 50]. In this study we use IHC to determine the distribution of neurocan at the scaffold/injury site and parenchyma. Figure 7 shows the distribution of neurocan (red fluorescence) in the injured spinal cord control and pHEMA groups. Increased neurocan expression could be found in an area surrounding the lesion site. Interestingly, while neurocan expression was highest ventral to the lesion site in the lesion-only group, this area was the lowest in the pHEMA group (Fig. 7). There was a statistically significant difference between the lesion only and the pHEMA group in this area (0–400 μm, $P < 0.05$, Fig. 8). Furthermore, the region within the scaffold had very low levels of neurocan as measured by IHC.

4 Conclusion

In summary, this small lesion animal SCI model allowed us to investigate the cellular and ECM microenvironment surrounding a TE scaffold without inflicting a severe injury on the animal. While such lesion injuries are not widely perceived as clinically relevant, our goal was to develop an in vivo model that assesses the host tissue response to an implanted material. Our approach differs from other hemisection models in that we implant a volume that is over 10 times smaller than other studies and into a region of white matter only. Importantly, the SCI lesion was small and post-operative care of the animal could be kept to a minimum. While the pHEMA scaffold reduced astrocyte gliosis and production of the inhibitory ECM protein neurocan, it was also dorsally relocated at 6 days and pushed entirely out of the spinal cord after 28 days. This small lesion in vivo SCI model may allow us to understand host tissue response to implants for the comparison of various TE scaffolds.

Acknowledgments We appreciate the support from the Natural National Science Foundation of China (Grants 30970727 and 31070844). We appreciate the help from Professor Lisa Xu with accommodating the in vivo experiments, Dr Brook Farrugia for SEM of the PCL electrospun membrane and Professor Alan Harvey for his instructive suggestions.

References

1. Fitch MT, Doller C, Combs CK, Landreth GE, Silver J. Cellular and molecular mechanisms of glial scarring and progressive cavitation: in vivo and in vitro analysis of inflammation-induced secondary injury after CNS trauma. J Neurosci. 1999;19(19):8182–98.
2. Fitch MT, Silver J. CNS injury, glial scars, and inflammation: inhibitory extracellular matrices and regeneration failure. Exp Neurol. 2008;209(2):294–301.
3. Dalton PD, Harvey AR, Oudega M, Plant GW. Tissue engineering of the nervous system. In: Van Blitterswijk C, Thompsen P, Lindhal A, Hubbell J, Williams DF, Cancedda R, et al., editors. Tissue engineering. Amsterdam: Academic Press; 2008. p. 611–47.
4. Schmidt CE, Leach JB. Neural tissue engineering: strategies for repair and regeneration. Annu Rev Biomed Eng. 2003;5:293–347. doi:10.1146/annurev.bioeng.5.011303.120731.
5. Straley KS, Foo CWP, Heilshorn SC. Biomaterial design strategies for the treatment of spinal cord injuries. J Neurotrauma. 2010;27(1):1–19. doi:10.1089/neu.2009.0948.
6. Basso DM, Beattie MS, Bresnahan JC, Anderson DK, Faden AI, Gruner JA, et al. MASCIS evaluation of open field locomotor scores: effects of experience and teamwork on reliability. J Neurotrauma. 1996;13(7):343–59.
7. Hulsebosch CE, Xu GY, Perez-Polo JR, Westlund KN, Taylor CP, McAdoo DJ. Rodent model of chronic central pain after spinal cord contusion injury and effects of gabapentin. J Neurotrauma. 2000;17(12):1205–17.
8. Tsai MC, Shen LF, Kuo HS, Cheng H, Chak KF. Involvement of acidic fibroblast growth factor in spinal cord injury repair processes revealed by a proteomics approach. Mol Cell Proteomics (MCP). 2008;7(9):1668–87. doi:10.1074/mcp.M800076-MCP200.
9. Scheff SW, Rabchevsky AG, Fugaccia I, Main JA, Lumpp JE Jr. Experimental modeling of spinal cord injury: characterization of a force-defined injury device. J Neurotrauma. 2003;20(2):179–93.

10. Jakeman LB, Guan Z, Wei P, Ponnappan R, Dzwonczyk R, Popovich PG, et al. Traumatic spinal cord injury produced by controlled contusion in mouse. J Neurotrauma. 2000;17(4):299–319.
11. Vanicky I, Urdzikova L, Saganova K, Cizkova D, Galik J. A simple and reproducible model of spinal cord injury induced by epidural balloon inflation in the rat. J Neurotrauma. 2001;18(12):1399–407.
12. Poon PC, Gupta D, Shoichet MS, Tator CH. Clip compression model is useful for thoracic spinal cord injuries—histologic and functional correlates. Spine. 2007;32(25):2853–9.
13. Mills CD, Hains BC, Johnson KM, Hulsebosch CE. Strain and model differences in behavioral outcomes after spinal cord injury in rat. J Neurotrauma. 2001;18(8):743–56. doi:10.1089/089771501316919111.
14. King VR, Hewazy D, Alovskaya A, Phillips JB, Brown RA, Priestley JV. The neuroprotective effects of fibronectin mats and fibronectin peptides following spinal cord injury in the rat. Neuroscience. 2010;168(2):523–30. doi:10.1016/j.neuroscience.2010.03.040.
15. Khatun F, King V, Alovskaya A, Brown RA, Priestley JV. Fibronectin based biomaterials as a treatment for spinal cord injury. Tiss Eng. 2007;13(7):1697.
16. Itosaka H, Kuroda S, Shichinohe H, Yasuda H, Yano S, Kamei S, et al. Fibrin matrix provides a suitable scaffold for bone marrow stromal cells transplanted into injured spinal cord: a novel material for CNS tissue engineering. Neuropathology. 2009;29(3):248–57. doi:10.1111/j.1440-1789.2008.00971.x.
17. Bakshi A, Fisher O, Dagci T, Himes BT, Fischer I, Lowman A. Mechanically engineered hydrogel scaffolds for axonal growth and angiogenesis after transplantation in spinal cord injury. J Neurosurg Spine. 2004;1(3):322–9.
18. Kubinova S, Horak D, Hejcl A, Plichta Z, Kotek J, Proks V, et al. SIKVAV-modified highly superporous PHEMA scaffolds with oriented pores for spinal cord injury repair. J Tiss Eng Regen Med. 2013;. doi:10.1002/term.1694.
19. Giannetti S, Lauretti L, Fernandez E, Salvinelli F, Tamburrini G, Pallini R. Acrylic hydrogel implants after spinal cord lesion in the adult rat. Neurol Res. 2001;23(4):405–9.
20. Stokols S, Sakamoto J, Breckon C, Holt T, Weiss J, Tuszynski MH. Templated agarose scaffolds support linear axonal regeneration. Tiss Eng. 2006;12(10):2777–87.
21. Stokols S, Tuszynski MH. Freeze-dried agarose scaffolds with uniaxial channels stimulate and guide linear axonal growth following spinal cord injury. Biomaterials. 2006;27(3):443–51. doi:10.1016/j.biomaterials.2005.06.039.
22. Teng YD, Lavik EB, Qu XL, Park KI, Ourednik J, Zurakowski D, et al. Functional recovery following traumatic spinal cord injury mediated by a unique polymer scaffold seeded with neural stem cells. Proc Natl Acad Sci USA. 2002;99(14):9606. doi:10.1073/pnas.112189299.
23. Kim H, Tator CH, Shoichet MS. Chitosan implants in the rat spinal cord: biocompatibility and biodegradation. J Biomed Mater Res Part A. 2011;97A:396–404.
24. Dalton PD, Klee D, Moller M. Electrospinning with dual collection rings. Polymer. 2005;46(3):611–4. doi:10.1016/j.polymer.2004.11.075.
25. Xu CY, Inai R, Kotaki M, Ramakrishna S. Electrospun nanofiber fabrication as synthetic extracellular matrix and its potential for vascular tissue engineering. Tiss Eng. 2004;10(7–8):1160–8. doi:10.1089/ten.2004.10.1160.
26. Chirila TV, Higgins B, Dalton PD. The effect of synthesis conditions on the properties of poly(2-hydroxyethyl methacrylate) sponges. Cell Polym. 1998;17(3):141–62.
27. Iannotti C, Zhang YP, Shields LB, Han Y, Burke DA, Xu XM, et al. Dural repair reduces connective tissue scar invasion and cystic cavity formation after acute spinal cord laceration injury in adult rats. J Neurotrauma. 2006;23(6):853–65. doi:10.1089/neu.2006.23.853.
28. Gelain F, Panseri S, Antonini S, Cunha C, Donega M, Lowery J, et al. Transplantation of nanostructured composite scaffolds results in the regeneration of chronically injured spinal cords. ACS Nano. 2011;5(1):227–36. doi:10.1021/nn102461w.
29. Schnell L, Fearn S, Klassen H, Schwab ME, Perry VH. Acute inflammatory responses to mechanical lesions in the CNS: differences between brain and spinal cord. Eur J Neurosci. 1999;11(10):3648–58.
30. Jain A, Kim YT, McKeon RJ, Bellamkonda RV. In situ gelling hydrogels for conformal repair of spinal cord defects, and local delivery of BDNF after spinal cord injury. Biomaterials. 2006;27(3):497–504. doi:10.1016/j.biomaterials.2005.07.008.
31. Liu T, Houle JD, Xu JY, Chan BP, Chew SY. Nanofibrous collagen nerve conduits for spinal cord repair. Tiss Eng Part A. 2012;18(9–10):1057–66. doi:10.1089/ten.tea.2011.0430.
32. King VR, Phillips JB, Hunt-Grubbe H, Brown R, Priestley JV. Characterization of non-neuronal elements within fibronectin mats implanted into the damaged adult rat spinal cord. Biomaterials. 2006;27(3):485–96. doi:10.1016/j.biomaterials.2005.06.033.
33. Bamber NI, Li HY, Aebischer P, Xu XM. Fetal spinal cord tissue in mini-guidance channels promotes longitudinal axonal growth after grafting into hemisected adult rat spinal cords. Neural Plast. 1999;6(4):103–21.
34. Bamber NI, Li HY, Lu XB, Oudega M, Aebischer P, Xu XM. Neurotrophins BDNF and NT-3 promote axonal re-entry into the distal host spinal cord through Schwann cell-seeded mini-channels. Eur J Neurosci. 2001;13(2):257–68.
35. Novikov LN, Novikova LN, Mosahebi A, Wiberg M, Terenghi G, Kellerth JO. A novel biodegradable implant for neuronal rescue and regeneration after spinal cord injury. Biomaterials. 2002;23(16):3369–76.
36. Teng YD, Lavik EB, Qu XL, Park KI, Ourednik J, Zurakowski D, et al. Functional recovery following traumatic spinal cord injury mediated by a unique polymer scaffold seeded with neural stem cells. Proc Natl Acad Sci USA. 2002;99(5):3024–9. doi:10.1073/pnas.052678899.
37. Bramlett HM. Sex differences and the effect of hormonal therapy on ischemic brain injury. Pathophysiology. 2005;12(1):17–27. doi:10.1016/j.pathophys.2005.02.009.
38. Roof RL, Hall ED. Gender differences in acute CNS trauma and stroke: neuroprotective effects of estrogen and progesterone. J Neurotrauma. 2000;17(5):367–88.
39. Crawford GJ, Chirila TV, Vijayasekaran S, Dalton PD, Constable IJ. Preliminary evaluation of a hydrogel core-and-skirt keratoprosthesis in the rabbit cornea. J Refract Surg. 1996;12(4):525–9.
40. Hicks C, Crawford G, Chirila T, Wiffen S, Vijayasekaran S, Lou X, et al. Development and clinical assessment of an artificial cornea. Prog Retinal Eye Res. 2000;19(2):149–70. doi:10.1016/s1350-9462(99)00013-0.
41. Fleming JC, Norenberg MD, Ramsay DA, Dekaban GA, Marcillo AE, Saenz AD, et al. The cellular inflammatory response in human spinal cords after injury. Brain. 2006;129(Pt 12):3249–69. doi:10.1093/brain/awl296.
42. Pekny M, Pekna M. Astrocyte intermediate filaments in CNS pathologies and regeneration. J Pathol. 2004;204(4):428–37. doi:10.1002/Path.1645.
43. Faulkner JR, Herrmann JE, Woo MJ, Tansey KE, Doan NB, Sofroniew MV. Reactive astrocytes protect tissue and preserve function after spinal cord injury. J Neurosci. 2004;24(9):2143–55. doi:10.1523/Jneurosci.3547-03.2004.
44. Lu YB, Iandiev I, Hollborn M, Korber N, Ulbricht E, Hirrlinger PG, et al. Reactive glial cells: increased stiffness correlates with increased intermediate filament expression. FASEB J. 2011;25(2):624–31. doi:10.1096/Fj.10-163790.

45. Woerly S, Petrov P, Sykova E, Roitbak T, Simonova Z, Harvey AR. Neural tissue formation within porous hydrogels implanted in brain and spinal cord lesions: ultrastructural, immunohistochemical, and diffusion studies. Tiss Eng. 1999;5(5):467–88.
46. Fuhrmann T, Hillen LM, Montzka K, Woltje M, Brook GA. Cell–cell interactions of human neural progenitor-derived astrocytes within a microstructured 3D-scaffold. Biomaterials. 2010;31(30):7705–15. doi:10.1016/j.biomaterials.2010.06.060.
47. Spilker MH, Yannas IV, Kostyk SK, Norregaard TV, Hsu HP, Spector M. The effects of tubulation on healing and scar formation after transection of the adult rat spinal cord. Restor Neurol Neurosci. 2001;18(1):23–38.
48. Spilker MH, Yannas IV, Hsu HP, Norregaard TV, Kostyk SK, Spector M. The effects of collagen-based implants on early healing of the adult rat spinal cord. Tiss Eng. 1997;3(3):309–17.
49. Asher RA, Morgenstern DA, Fidler PS, Adcock KH, Oohira A, Braistead JE, et al. Neurocan is upregulated in injured brain and in cytokine-treated astrocytes. J Neurosci. 2000;20(7):2427–38.
50. Properzi F, Carulli D, Asher RA, Muir E, Camargo LM, van Kuppevelt TH, et al. Chondroitin 6-sulphate synthesis is up-regulated in injured CNS, induced by injury-related cytokines and enhanced in axon-growth inhibitory glia. Eur J Neurosci. 2005;21(2):378–90. doi:10.1111/j.1460-9568.2005.03876.x.